

Primary standardization of ^{224}Ra activity by liquid scintillation counting

Elisa Napoli,^{1,2,3,4} Jeffrey T. Cessna,¹ Ryan Fitzgerald,¹ Leticia Pibida,¹ Ronald Collé,¹

Lizbeth Laureano-Pérez,¹ Brian E. Zimmerman,¹ and Denis E. Bergeron^{1*}

¹Physical Measurement Laboratory, National Institute of Standards and Technology,
Gaithersburg, MD 20899-8462, USA

²Oncoinvent AS, Oslo, Norway

³Institute of Clinical Medicine, University of Oslo, Oslo, Norway

⁴Department of Radiation Biology, Institute for Cancer Research, Oslo University Hospital,
Oslo, Norway

[*denis.bergeron@nist.gov](mailto:denis.bergeron@nist.gov)

Abstract

A standard for activity of ^{224}Ra in secular equilibrium with its progeny has been developed, based on triple-to-double coincidence ratio (TDCR) liquid scintillation (LS) counting. The standard was confirmed by efficiency tracing and $4\pi\alpha\beta(\text{LS})-\gamma(\text{NaI}(\text{Tl}))$ anticoincidence counting, as well as by $4\pi\gamma$ ionization chamber and NaI(Tl) measurements. Secondary standard ionization chambers were calibrated with an expanded uncertainty of 0.62 % ($k = 2$). Calibration settings were also determined for a 5 mL flame-sealed ampoule on several commercial reentrant ionization chambers (dose calibrators).

Keywords

TDCR; liquid scintillation; anticoincidence counting; efficiency tracing; alpha therapy; activity calibration

1. Introduction

Radium-224 (historically known as Thorium-X), daughter of ^{228}Th , is an alkaline earth element with a half-life of 3.631(2) d (Bé et al., 2004; DDEP, 2018). Radium-224 has a complex decay chain with six short-lived daughter radionuclides, including the emission of four energetic alpha particles (Figure 1). The first ^{224}Ra daughter is ^{220}Rn (half-life 55.8(3) s (Bé et al., 2004; DDEP, 2018)), followed by ^{212}Pb , which has the longest half-life of 10.64(1) h (Bé et al., 2004; DDEP, 2018) in the decay scheme. In recent years, ^{224}Ra has been used as an effective tracer for monitoring coastal water mixing processes (Moore, 2000; 2003), but historically, most research surrounding ^{224}Ra has been medically motivated. The first isotopic separation of ^{224}Ra was reported in 1900 by Rutherford and Soddy (1900) and the first medical use was registered in 1912 by two independent scientists in Germany: Pappenheim and Bickel. The first studied oral administration of ^{224}Ra in patients suffering from anemia and leukemia (Pappenheim and Plesch, 1912); the second researched intravenous injection of ^{224}Ra in patients affected by ankylosing spondylitis (Bickel, 1912), an inflammatory disease of the vertebral column. Numerous other medical applications for ^{224}Ra were researched, especially before and immediately after World War II. Poor knowledge of the effects of ionizing radiation, particularly on growing and developing tissues, likely account for many of the very serious reported side-effects (e.g., Spiess, 2002). Difficulties were probably also compounded by the lack of a reliable method for measuring activity, which was initially calculated in electrostatic units, an obsolete unit used until 1969 for ^{224}Ra medical dosage (Wick and Gössner, 1993). More recently, a suspension of injectable calcium carbonate microparticles labeled with ^{224}Ra has shown promise in preclinical studies for treatment of cavitary micro-metastatic cancer (Westrøm et al., 2018a; 2018b).

This therapeutic use of ^{224}Ra exploits the high energy and short range of alpha particles to induce non-repairable double-strand DNA breaks with minimal toxicity to surrounding healthy tissues. Prior to commencing clinical trials, it is essential to develop a radioactivity standard for ^{224}Ra to assure consistent dosage administration and to accurately calculate dose-response relationships.

We report here a series of primary activity determinations using several liquid scintillation (LS) counting-based methods. Triple-to-double coincidence ratio (TDCR) LS counting, CIEMAT-NIST efficiency tracing (CNET) with tritium, and live-timed $4\pi\alpha\beta(\text{LS})-\gamma(\text{NaI})$ anticoincidence counting (LTAC) were all employed (Broda et al., 2007; Bobin, 2007; Fitzgerald et al., 2015). These measurements were complemented by Monte Carlo simulations to model instrument responses, ensuring appropriate corrections and establishing theoretical links with $4\pi\gamma$ ionization chamber or NaI(Tl) measurements. Through gamma-ray spectrometry with high-purity germanium (HPGe) detectors and ionization chamber measurements, we place our activity measurements in context with previous and contemporary efforts.

2. Material and methods

2.1. Source preparation

The solutions for all experiments were supplied by Oncoinvent AS (Oslo, Norway).¹ In Experiment 1 (E1), the solution was shipped directly to NIST from Oncoinvent. In Experiments 2 through 4 (E2 - E4) the material was prepared and shipped by Oak Ridge National Laboratory (Oak Ridge, Tennessee, USA). In all cases, the solutions consisted of

¹ Certain commercial equipment, instruments, or materials are identified in this paper to foster understanding. Such identification does not imply recommendation by the National Institute of Standards and Technology, nor does it imply that the materials or equipment identified are necessarily the best available for the purpose.

$^{224}\text{RaCl}_2$ in 1 mol/L HCl. All solutions were determined to be free of gamma-ray emitting impurities by HPGe spectrometry measurements.

E1 established the validity of gravimetric links by demonstrating that the 1 mol/L HCl solution affords loss-free transfers (see Section 3.1). E2 - E4 linked liquid scintillation (LS)-based assays and ionization chamber (IC) calibrations to establish and preserve a primary activity standard.

In all experiments, LS and IC sources were prepared by serial gravimetric dilutions of a common master solution. Dilutions were carried out with 1.1 mol/L HCl. All sources were prepared gravimetrically using the aspirating pycnometer method (Sibbens and Altzitzoglou, 2007); when practicable, both dispensed and contained masses were measured for confirmation. LS sources were prepared with Ultima Gold (UG) or Ultima Gold AB (UGAB; PerkinElmer, Wesley, MA, USA) with aqueous fractions (f_{aq} , by volume) of 0.05 for UG and 0.07 for UGAB. Past experience (e.g., Bergeron, 2012) has shown these compositions to be generally stable. In E2 and E4, 1.1 mol/L HCl was used to bring the total aqueous fraction to the desired value; in E3, water was used.

2.2. Primary methods

All nuclear and atomic data used as input for the analysis of experimental data were taken from the Decay Data Evaluation Project (Bé et al., 2004; DDEP, 2018). Table 1 shows the evaluation date for ^{224}Ra and its progeny, along with the half-lives used and the equilibrium activity ratios derived from the Bateman equation (Bateman, 1908).

The primary activity standardization was achieved with three liquid scintillation-based methods: triple-to-double coincidence ratio (TDCR) counting, CIEMAT/NIST efficiency tracing (CNET) with ^3H , and live-timed $4\pi\alpha\beta(\text{LS})-\gamma(\text{NaI})$ anticoincidence counting (LTAC). Data used for the standardization were acquired with sources at secular equilibrium (> 6 d

after separation) so that decay correction to a common reference time was achieved using the half-life for ^{224}Ra (Table 1). For all methods, it was assumed that the short-lived ($T_{1/2} = 300(2)$ ns) ^{212}Po daughter and its ^{212}Bi parent are detected with a combined efficiency of 100 %. Kossert and Nähle (2011) discuss this phenomenon in their treatment of the same decay chain. In most instances, ^{212}Po decays within the deadtime triggered by ^{212}Bi decay ($\epsilon_{\text{Bi}} > 0.995$). In the rare instances that ^{212}Bi is not detected, its α -emitting ^{212}Po daughter ($\epsilon_{\text{Po}} = 1$) is, so that $\epsilon_{\text{Bi+Po}} = 1$. This assumption was confirmed experimentally (Section 2.2.1). The case is similar to our previous treatment of the $^{213}\text{Po} + ^{213}\text{Bi}$ pair in the decay chain of ^{229}Th (Fitzgerald et al., 2010), but ^{213}Po has a longer lifetime (3.70(5) μs ; Bé, 2008) so that in multiple PMT systems there is a greater probability of daughter decay beyond the coincidence resolving time that defines PMT coincidence events (see Kossert et al., 2014).

2.2.1. TDCR

Sources for TDCR counting were prepared in standard (clear) 22 mL glass scintillation vials with foil-lined caps. The foil-lined caps are intended to assure no loss of ^{220}Rn , although the high solubility of Rn in the LS cocktails is expected to prevent diffusion from the cocktail into the headspace. LS efficiencies for α -decays were assumed to be 100 %. Efficiency calculations for β -decaying progeny of ^{224}Ra were carried out with the MICELLE2 code (Kossert and Grau Carles, 2010) using the relevant decay data evaluation project (DDEP) data. The code was modified to allow for $Z > 82$ and simplified decay schemes were used with branch normalizations chosen to assign “missing” decays to similar cascades (Table 2). Measurements were performed on the NIST TDCR counter, which has been described previously (Zimmerman et al., 2004). Data were acquired with a home-built FPGA-based system that has been validated against a MAC3 (Bouchard and Cassette, 2000) unit. An extending-type deadtime of 50 μs was imposed and the coincidence resolving time (τ) was varied as described presently.

The simplified decay scheme assumes 100 % efficiency for $^{212}\text{Po} + ^{212}\text{Bi}$ (see section 2.2). To check for deviations from expected behavior, counts were taken with variable τ using the darkest available gray filter to reduce counting efficiency, exacerbating the problem of missed coincidences when a pulse is detected by just one or two PMTs during τ (see, e.g., Kossert et al., 2014). The range of τ started at 10 ns (known to be too short to capture all true coincidences on our system due to photomultiplier tube timing characteristics and variances in the duration of light production in the scintillation process) and was increased to 500 ns. The observed logical sum of doubles (LSD) rate was consistent for $\tau > 20$ ns (Figure 2). Data for the standardization were collected with $\tau = 150$ ns. The problem of missed coincidences is expected to contribute a small shift in the total counting efficiency, but even with the darkest gray filter, only a ≈ 0.01 % difference between $\tau = 50$ ns and $\tau = 150$ ns is expected due to the 300 ns half-life of ^{212}Po . This would not be detectable in Figure 2, but is accounted in the uncertainty evaluation.

For the activity determinations, counting efficiency was varied with gray filters, achieving a triple-to-double coincidence ratio (R) range of (0.986 to 0.992) and corresponding to a logical sum of doubles counting efficiency (ϵ_D) range of (5.05 to 5.66) counts per ^{224}Ra decay, according to the MICELLE2 model and Bateman equations solution. No trending with efficiency was seen in the calculated activities.

2.2.2. CIEMAT/NIST efficiency tracing (CNET)

Sources for CNET were prepared in standard (clear) 22 mL glass scintillation vials with foil-lined caps. Efficiency calculations relied on the same MICELLE2 model used for TDCR (see section 2.2.1 and Table 2). For CNET, efficiency variation was achieved by chemical quenching with nitromethane and all ^{224}Ra sources were measured against matched ^3H sources. The ^3H sources were prepared using a gravimetric dilution of NIST tritiated-water (Hydrogen-3) standard SRM 4927g (NIST 2015; Collé et al., 2016).

Samples were measured on a Beckman Coulter LS6500 (Beckman Coulter, Fullerton, CA, USA) and a Packard Tri-Carb 4910 (PerkinElmer, Waltham, MA, USA), with consistent results. The samples covered a range of ^3H counting efficiencies ($\epsilon_{\text{H-3}}$) of (0.28 to 0.46) counts per ^3H decay, corresponding to a range of ^{224}Ra counting efficiencies ($\epsilon_{\text{Ra-224}}$) of (5.66 to 5.68) counts per ^{224}Ra decay. Over this range, our calculated ^{224}Ra efficiencies were 0.023 % to 0.035 % lower than those estimated using the polynomial given by Kossert and Nähle (2011). Calculated activities showed no trending with time or traced efficiency.

2.2.3. Live timed anticoincidence (LTAC) counting

Sources for LTAC counting at NIST are prepared in custom-built glass hemispheres sealed with epoxy. The NIST LTAC system consists of a single PMT which is optically coupled to the hemisphere source and placed inside a well-type NaI(Tl) detector (Lucas, 1998; Fitzgerald and Schultz, 2008). Data were collected in both analog and digital (list mode) configurations, with consistent results. The analyses discussed here used the analog data.

Three anticoincidence gates (G1, G2, and G3) were set to cover peaks in the NaI(Tl) spectrum arising from both beta and alpha emitters (Figure 3) to assure optimal monitoring of the LS efficiencies. These efficiencies are determined from the anticoincidence data from each gate as LS inefficiencies (Y_1 , Y_2 , and Y_3 ; *vide infra*) and varied experimentally by changing the lower level discriminator in the LS channel. By plotting Y vs. N_{LS} (where N_{LS} is the LS count rate) an extrapolation over an appropriate linear region can be used to determine the count rate at perfect LS efficiency ($Y = 0$).

Simulations in GEANT4 (Agostinelli et al., 2003) were used to examine gate sensitivity, determine gate weights to achieve extrapolations with good linearity and high-fidelity intercepts, and to calculate correction factors to be applied to extrapolation intercepts. Using an “effective inefficiency” (Y_{eff}), calculated from a weighted combination of contributions from multiple gates, is a well-established method for achieving robust extrapolations and

assuring sensitivity to all decay types (Fitzgerald et al., 2015). Applying Monte Carlo correction factors to the intercept of the Y_{eff} versus N_{LS} (where N_{LS} is the LS count rate) curve is also now a well-established method for accounting for deviations from linearity in LTAC data; the Monte Carlo model used for these studies was recently described by Bergeron and Fitzgerald (2018).

Gate 1 (G1) was set to cover the 186 keV to 257 keV range, so that the 241 keV γ -ray from ^{224}Ra decay and the 239 keV γ -ray from ^{212}Pb decay were both captured. At secular equilibrium, most of the intensity in this gate comes from ^{212}Pb $\beta_{0,2}$ - γ decay. The relatively flat curve for Y_1 in Figure 4 (black trace) reflects the high counting efficiency for α and β^- ($E_{\text{max}} = 331$ keV) particles.

Gate 2 (G2) covered 525 keV to 1255 keV, where the peaks are mostly from ^{212}Bi and ^{208}Tl , along with significant contributions from summing. Thus, Y_2 includes both α - and β^- -decay contributions, providing a sensitive measure of LS counting efficiency (red trace, Figure 4).

Gate 3 (G3) covered 2420 keV to 3055 keV, capturing the 2615 keV γ -ray from ^{208}Tl decay. The gray trace in Figure 4 shows that G3 provides a good measure of the LS counting efficiency for the high energy (almost exclusively > 1 MeV) β^- particles. The significant overlap between the Y_2 and Y_3 curves in Figure 4 is expected since the same β^- decays for ^{208}Tl are monitored by both gates.

The three gates sampled in these experiments yield inefficiency extrapolations with nearly convergent intercepts (Figure 4). Applying correction factors calculated from the Monte Carlo simulations improved accord between intercepts obtained with different gates (see Section 3.3.3). For the final LTAC activity, an effective inefficiency ($Y_{\text{eff}} = 0.29*Y_1 + 0.67*Y_2 + 0.04*Y_3$) was used to achieve a linear extrapolation. These coefficients were determined from

the Monte Carlo simulations, using a least squares approach to find the gate weights that give the best linear fit.

2.3. Secondary methods

2.3.1. Ionization chamber calibration

In each experiment, several ampoules were measured on reentrant ionization chambers (ICs) in order to establish calibration factors that will be used for subsequent calibrations of ^{224}Ra . The ampoule geometry is defined as 5 mL of solution in a 5 mL flame-sealed NIST standard ampoule. While measurements were initiated shortly after the ampoules were prepared, allowing the observation of the ingrowth of progeny, the calibration factors were determined after the solutions had reached secular equilibrium (> 6 d after separation). In the NIST automated ionization chamber (AutoIC; Fitzgerald 2010), measurements of ^{224}Ra ampoules were bracketed by measurements of a ^{226}Ra reference source (RRS). The AutoIC calibration factor (K_{AIC}) is expressed as a function of the ratio of responses measured for ^{224}Ra and the RRS. Finally, using an energy-dependent response curve derived empirically for the AutoIC, theoretical values for K_{AIC} were calculated based on the expected γ -ray emissions from the ^{224}Ra decay chain.

The Vinten 671 ionization chamber (VIC) at NIST is related to sister chambers at other national metrology institutes, including the National Physical Laboratory (NPL) in Teddington, UK, allowing for indirect comparison of activity standards (see, e.g., Bergeron and Cessna, 2018). Calibration factors for the VIC (K_{VIC}) are expressed directly as a function of current in units of pA/MBq. Measurements of the RRS are performed routinely (at least daily during a calibration campaign) to monitor the performance of the VIC and assure response constancy over time.

2.3.2. Gamma-ray spectrometry measurements

In each experiment, ampoules were measured on high-purity germanium (HPGe) detectors to check for photon-emitting radionuclidic impurities, confirm secular equilibrium, and estimate solution activities based on DDEP gamma emission probabilities (P_g). These data will be used in conjunction with the primary activity measurements to derive new gamma-emission probabilities (to be presented in a separate publication).

Samples were also measured on a Wallac Wizard 2480 automatic NaI(Tl) well-type counter. We have developed a Monte Carlo model in GEANT4 for this detector based on specifications provided by the manufacturer. Our model has been benchmarked with ^{18}F measurements and found to be consistent with the model described by Lodge et al. (2015). The ^{224}Ra sources were measured in ampoules in custom centering sleeves and with an open counting window (nominally 20 keV to 2000 keV).

3. Results

3.1. Assuring loss-free transfers

The sources measured by primary and secondary methods were all linked to a common solution by mass. Thus, the integrity of all calibrations depends critically on our ability to transfer solutions from one container to another without changing the activity concentration. Experiment 1 (E1) was dedicated to establishing that loss-free transfers of the $^{224}\text{RaCl}_2$ solution were possible. Two ampoules were initially prepared from a common master solution. One of them (A2) was repeatedly opened and transferred to a new ampoule, while the other (A1) was kept as a control. Measuring the ampoules on the VIC revealed that A1 and A2 (and its daughter ampoules, A2-T1 and A2-T2) gave consistent instrument responses (in pA/g). Figure 5 shows that, while the VIC response is gradually increasing over the course of 2 days as the solution reaches secular equilibrium, the A1 and A2 responses are equivalent. In addition, where possible, all gravimetric dilution factors in all experiments were confirmed radiometrically. In all cases, dilution factors agreed within uncertainties.

3.2. Impurities

In each experiment, ampoules were measured on high-purity germanium (HPGe) detectors to look for photon-emitting impurities. No impurities were detected within the following photon emission rates (for a 5 mL ampoule containing approximately 1.8 MBq of ^{224}Ra at the time of HPGe measurement):

$25 \text{ keV} < E < 235 \text{ keV}$	280 s^{-1}
$245 \text{ keV} < E < 295 \text{ keV}$	380 s^{-1} (skipped 239 keV to 241 keV lines)
$310 \text{ keV} < E < 500 \text{ keV}$	470 s^{-1} (skipped 300 keV line)
$520 \text{ keV} < E < 570 \text{ keV}$	500 s^{-1} (skipped 511 keV line)
$590 \text{ keV} < E < 720 \text{ keV}$	470 s^{-1} (skipped 583 keV line)
$740 \text{ keV} < E < 850 \text{ keV}$	480 s^{-1} (skipped 727 keV line)
$870 \text{ keV} < E < 1580 \text{ keV}$	680 s^{-1} (skipped 861 keV line)
$1600 \text{ keV} < E < 2000 \text{ keV}$	1200 s^{-1} (skipped 1593 keV line)

At later times (i.e., after several ^{224}Ra half-lives), the presence of ^{228}Th was observed, but never at levels that significantly affected the measurements ($f_{\text{Th-228}} = A_{\text{Th-228}}/A_{\text{Ra-224}} < 0.002 \%$ at the separation time). No corrections were made.

3.3. Primary activity determinations

3.3.1. Triple-to-double coincidence ratio (TDCR) counting

The TDCR results were adopted for the primary activity standard for ^{224}Ra . Table 3 provides a detailed uncertainty budget. In E2, the combined standard uncertainty was mostly due to within- and between-insertion (where a single insertion refers to placing the source into the counter once) measurement variability. The results in E3 were comparable, but with the activity concentration appearing to trend down slightly with time (embodied in both the counting uncertainty and the between-source variance, since one source was counted after the other). Such a trend could arise from cocktail instability due to the use of water (instead of 1.1

mol/L HCl, as in E2) in the cocktail preparations. By diluting the acid content in the aqueous phase of the cocktails, the solubility of ^{224}Ra and its progeny would be reduced. However, the CNET data do not show an analogous trend over the same time period (Figure 6; Section 3.3.2). Finally, in E3, a much larger between-source uncertainty resulted in an overall larger combined standard uncertainty. With only two sources, it is not clear whether any specific anomaly accounts for the variance, but the magnitude is relatively small. The apparent cocktail instability in E3 motivated additional TDCR measurements in E4. Uncertainties in E4 were comparable to those in E2.

The calculated activities were relatively insensitive to nuclear data and efficiency model, giving a robust result with small combined standard uncertainty.

3.3.2. CIEMAT/NIST efficiency tracing (CNET)

The CNET results were considered confirmatory. Table 4 provides a detailed uncertainty budget. In E2, the within-cycle variance dominated the LS measurement precision uncertainty. In E3, between-cycle variance was of similar magnitude to within-cycle variance, contributing to significantly larger LS measurement precision uncertainty. This is consistent with the TDCR findings, except that the trending with time is absent. In addition, the E3 CNET measurements included two scintillants (Ultima Gold and Ultima Gold AB). The calculated activities were systematically higher for the Ultima Gold series, with $A_{\text{UG}}/A_{\text{UGAB}} = 1.0017(9)$ where the stated uncertainty is a standard deviation on the ratio determined from average activities on three measurement occasions. This cocktail-dependence is embodied in the LS measurement precision in Table 4. Finally, for both E2 and E3, model-dependency was estimated assuming a conservative 1 % uncertainty on the calculated β counting efficiencies.

3.3.3. Live timed anticoincidence (LTAC) counting

The Monte Carlo-corrected LTAC results were considered confirmatory. Table 5 shows how the Monte Carlo correction improved agreement between extrapolations with different gates.

Table 6 shows the detailed uncertainty budget for LTAC. In E2, the combined standard uncertainty was mostly due to counting statistics. In E3, the counting uncertainty was much smaller, but between-source uncertainty (which can capture statistical and systematic variances otherwise missed) was larger, resulting in a combined standard uncertainty of similar magnitude.

The intercepts were relatively insensitive to nuclear data, gate selection, extrapolation type, and inefficiency domains, bolstering confidence in the robustness of the LTAC result.

3.4. Links and calibrations

The massic activities determined by TDCR and LTAC in both E2 and E3 agreed to within the LTAC uncertainties (Table 7). The CNET results agreed with TDCR to within the expanded ($k = 2$) CNET uncertainties; the CNET activity was low relative to TDCR in E2 and high in E3.

Further confirmation of the TDCR-based activity standard came from the theoretical K_{AIC} and Monte Carlo-calculated NaI(Tl) well counter response. For both of these $4\pi\gamma$ methods, the calculated activities agreed with TDCR to $< 0.2\%$, much better than the estimated model uncertainties ($> 1.4\%$).

The activities calculated from HPGe measurements, using the $\gamma_{1,0}(\text{Rn})$ (241 keV) line with the DDEP recommended value of 4.12(4) photons per 100 disintegrations (Bé et al., 2004; DDEP, 2018), are consistently biased (Table 7). We are collecting and analyzing additional data, but these initial measurements appear to be consistent with the set of historical data, but not the recommended value. The most recent P_g determinations, with smaller uncertainties (especially Gehrke et al., 1984), receive substantial weight in the data evaluation, making many historical measurements (especially Peghaire, 1969; Dalmasso, 1972; Kurcewicz et al.,

1977; and Sadasivan and Raghunath, 1982), and our measurements, inconsistent with the DDEP-recommended P_g (Bé et al., 2004; DDEP, 2018).

Good between-method agreement was accompanied by good between-experiment agreement as established via IC responses. VIC and AutoIC responses were consistent within uncertainties, indicating accord among the three TDCR determinations (Table 7).

The AutoIC data in Table 7 are presented using the theoretically calculated calibration factor (K_{AIC}). An experimental K_{AIC} was determined from results of E2, E3, and E4, with an uncertainty component reflecting the experiment-to-experiment variance (Table S1). The final adopted value for 5 mL of a 1 mol/L HCl solution of ^{224}Ra in equilibrium with its progeny in a NIST standard 5 mL flame sealed ampoule agrees with the theoretically determined K_{AIC} ($K_{AIC,expt} / K_{AIC,theo} = 1.0009$) to well-within the estimated 1.4 % uncertainty on the theoretical value.

The VIC calibration factor (K_{VIC}) determined from the TDCR activity in each experiment was consistent within uncertainties (Table 7). Weighted and unweighted averages were identical within the significant figures. Moreover, weighted and unweighted averages that included both TDCR and LTAC results were identical within the significant figures. The final uncertainty analysis (Table S2) combines the TDCR results from E2, E3, and E4, with an uncertainty component reflecting experiment-to-experiment variance. The final adopted value for 5 mL of a 1 mol/L HCl solution of ^{224}Ra in equilibrium with its progeny in a NIST standard 5 mL flame-sealed ampoule is $K_{VIC} = 13.97(9)$ pA/MBq ($k = 2$). An informal comparison of K_{VIC} values with colleagues at the NPL indicates accord between our standards.

Measurements were also performed on several Capintec (Florham Park, New Jersey, USA) radionuclide calibrators. The calibration number (“dial setting”) expected to return the correct

(according to the contemporary TDCR measurements) activity for a 5 mL ampoule in each instrument was determined using the calibration curve method (Zimmerman and Cessna, 2000). Uncertainties were estimated by combining components for the uncertainty on the standard activity with the uncertainty due to the half-life corrections ($< 0.1\%$), the uncertainty due to the calibration curve fit (0.2% to 0.7% , encompassing measurement repeatability), and the experiment-to-experiment variance (0.1% to 0.5%). Table 8 gives a summary of the dial settings determined for the NIST-maintained calibrators in the ampoule geometry.

4. Conclusions

NIST has developed a radioactivity standard for ^{224}Ra in equilibrium with its progeny. The primary activity standard is based on triple-to-double coincidence ratio (TDCR) liquid scintillation counting, with efficiencies for the ^{212}Pb and ^{208}Tl daughters calculated with the MICELLE2 code. The standard was confirmed by CIEMAT/NIST efficiency tracing (CNET) and live-timed anticoincidence (LTAC) counting; results agreed within uncertainties.

The standard was further confirmed via comparison of theoretical and measured responses of ionization chambers and an automatic NaI(Tl) well counter. An informal comparison of Vinten 671 ionization chamber (VIC) calibration factors (K_{VIC}) with the NPL indicated accord between UK and US standards.

The standard was transferred to several ionization chambers, including the NIST AutoIC, allowing future calibrations at NIST with an expanded uncertainty of 0.62% ($k = 2$). This standard will form the basis for clinically significant calibrations in other chemical forms and in other measurement geometries. Future drug products based on, e.g., labeled microparticles, will present unique measurement challenges, requiring specific calibration and/or correction factors to account for attenuation and geometry effects. Efforts are underway at NIST to develop measurement strategies and models for these challenging cases. These will assure

future therapeutic interventions are administered with reliable dosage measurements, providing a sound basis for establishing dose-response relationships.

Acknowledgements

We are grateful to John Keightley (National Physical Laboratory, UK) for frequent and ongoing enthusiastic and collaborative discussions. This work was funded in part by Oncoinvent AS, Norway. EN is employed by and owns stock in Oncoinvent. EN was supported by the Industrial PhD project n.259820/O30 of the Norwegian National Research Council.

References

- Agostinelli, S., Allison, J., Amako, E., et al., 2003. "GEANT4 – a simulation toolkit." Nucl. Inst. Methods Phys Res A 506, 250-303.
- Bateman, H, 1908. "The solution of a system of differential equations occurring in the theory of radio-active transformations." Proc. Cambridge Phil. Soc. 15, 423-427.
- Bé, M.-M., Chisté, V., Dulieu, C., Browne, E., Chechev, V., Kuzmenko, N., Helmer, R., Nichols, A., Schönfeld, E., Dersch, R., 2004. Table of Radionuclides (Vol. 2 – A = 151 to 242). Monographie BIPM-5.
- Bé, M.-M., Chisté, V., Dulieu, C., Browne, E., Cechev, V., Kuzmenko, N., Kondev, F., Luca, A., Galán, M., Pearce, A., Huang, X., 2008. Table of Radionuclides (Vol. 4 – A = 133 to 252). Monographie BIPM-5.
- Bergeron, D.E., 2012. "Determination of micelle size in some commercial liquid scintillation cocktails." Appl. Radiat. Isot. 70, 2164-2169.
- Bergeron, D.E., Cessna, J.T., 2018. "An update on 'dose calibrator' settings for nuclides used in nuclear medicine." Nucl. Med. Commun. 39, 500-504.

- Bergeron, D.E., Fitzgerald, R., 2018. "Monte Carlo modelling of live-timed anticoincidence (LTAC) counting for Cu-64." *Appl. Radiat. Isot.* 134, 280-285.
- Bickel, A., 1912. "Über Mesothorium, Thorium X- und Thoriumemanationstherapie." *Berl. klin Wochnschr* 17, 777-779.
- Bobin, C., 2007. "Primary standardization of activity using the coincidence method based on analogue instrumentation." *Metrologia* 44, S27-S31.
- Bouchard, J., Cassette, P., 2000. "MAC3: an electronic module for the processing of pulses delivered by a three photomultiplier liquid scintillation counting system." *Appl. Radiat. Isot.* 52, 669-672.
- Broda, R., Cassette, P., Kossert, K., 2007. "Radionuclide metrology using liquid scintillation counting." *Metrologia* 44, S36-S52.
- Collé, R., Laureano-Perez, L., Bergeron, D.E., 2016. "Comparison of tritiated-water standards by liquid scintillation for calibration of a new Standard Reference Material®." *Appl. Radiat. Isot.* 112, 38-49.
- Dalmasso, J., 1972. "Recherches sur le rayonnement gamma de quelques radioéléments naturels appartenant la famille du thorium." Ph.D. thesis, University of Nice.
- DDEP, accessed 2018: <http://www.lnhb.fr/nuclear-data/nuclear-data-table/>
- Fitzgerald, R., Schultz, M.K., 2008. "Liquid-scintillation-based anticoincidence counting of Co-60 and Pb-210." *Appl. Radiat. Isot.* 66, 937-940.
- Fitzgerald, R., 2010. "An automated ionization chamber for secondary radioactivity standards." *Appl. Radiat. Isot.* 68, 1507-1509.

- Fitzgerald, R., Collé, R., Laureano-Pérez, L., Pibida, L., Hammond, M.M., Nour, S., Zimmerman, B.E., 2010. "A new primary standardization of ^{229}Th ." *Appl. Radiat. Isot.* 68, 1303-1308.
- Fitzgerald, R., Bailat, C., Bobin, C., Keightley, J.D., 2015. "Uncertainties in $4\pi\beta\text{-}\gamma$ coincidence counting." *Metrologia* 52, S86-S96.
- Gehrke, R.J., Novick, V.J., Baker, J.D., 1984. " γ -ray emission probabilities for the ^{232}U decay chain." *Appl. Radiat. Isot.* 35, 581-589.
- Kossert, K., Nähle, O., 2011. "Activity determination of ^{228}Th by liquid scintillation counting." LSC2010, *Advances in Liquid Scintillation Spectrometry: Proceedings of the 2010 International Conference on Liquid Scintillation Spectrometry*, Paris, France, 6-10 September 2010, edited by Philippe Cassette, in *Radiocarbon*, the University of Arizona, Tuscon, Arizona, USA, ISBN 978-0-963831-7-7, 151-160.
- Kossert, K., Grau Carles, A., 2010. "Improved method for the calculation of the counting efficiency of electron-capture nuclides in liquid scintillation samples." *Appl. Radiat. Isot.* 68, 1482-1488.
- Kossert, K., Nähle, O.J., Janßen, H., 2014. "Activity determination of ^{229}Th by means of liquid scintillation counting." *Appl. Radiat. Isot.* 87, 274-281.
- Kurcewicz, W., Kaffrell, N., Trautmann, N., Plochocki, A., Zylicz, J., Matul, M., Stryczniewicz, K., 1977. "Collective states fed by weak α -transitions in the ^{232}U chain." *Nucl. Phys. A* 289, 1-14.
- Lucas, L.L., 1998. Calibration of the massic activity of a solution of Tc-99. *Appl. Radiat. Isot.* 49, 1061-1064.

- M.A. Lodge, D.P. Holt, P.E. Kinahan, D.F. Wong, R.L. Wahl, 2015. "Performance assessment of a NaI(Tl) gamma counter for PET applications with methods for improved quantitative accuracy and greater standardization." *Eur. J. Nucl. Med. Molec. Imag. Phys.* 2:11.
- Moore, W.S., 2000. "Determining coastal mixing rates using radium isotopes." *Cont. Shelf Res.* 20, 1993-2007.
- Moore, W.S., 2003. "Sources and fluxes of submarine groundwater discharge delineated by radium isotopes." *Biogeochemistry* 66, 75-93.
- National Institute of Standards and Technology (NIST), 2015. *Certificate for Standard Reference Material 4927g, Hydrogen-3 Radioactivity Standard*, NIST, Gaithersburg, MD, USA, November 2015.
- Pappenheim, A., Plesch, J., 1912. "Einige Ergebnisse über experimentelle und histologische Untersuchungen zur Wirkung des Thorium X auf den tierischen Organismus." *Berl. klin. Wochenschr.* 49, 1342.
- Peghaire, A., 1969. "Mesures précis d'intensités absolues de rayonnements γ pour des émetteurs α ." *Nucl. Instrum. Methods* 75, 66-70.
- Rutherford, E. I., Soddy, F., 1900. "A radio-active substance emitted from thorium compounds." *The London, Edinburgh, and Dublin Philosophical Magazine and Journal of Science*, 49,1-4.
- Sadasivan, S., Raghunath, V.M., 1982. "Determination of γ -ray emission probabilities in the decay of ^{228}Th and its daughters." *Nucl. Instrum. Methods* 196, 561-563.
- Sibbens, G., Altitzoglou, T., 2007. «Preparation of radioactive sources for radionuclide metrology.» *Metrologia* 44, S71-78.

- Spiess, H., 2002. "Peteosthor – a medical disaster due to Radium-224." *Radiat. Environ. Biophys.* 41, 163-172.
- Westrøm, S., Malenge, M., Jorstad, I.S., Napoli, E., Bruland, Ø.S., Bønsdorff, T.B., Larsen, R.H., 2018a. "Ra-224 labeling of calcium carbonate microparticles for internal α -therapy: Preparation, stability, and biodistribution in mice." *J. Label. Compd. Radiopharm.*, 61, 472-86.
- Westrøm, S., Bønsdorff, T. B., Bruland, Ø. S., & Larsen, R. H., 2018b. Therapeutic Effect of α -Emitting ^{224}Ra -Labeled Calcium Carbonate Microparticles in Mice with Intraperitoneal Ovarian Cancer. *Transl. Oncol.*, 11(2), 259-267.
- Wick, R.R., Gössner, W., 1993. "History and current uses of ^{224}Ra in ankylosing spondylitis and other diseases." *Environ. Int.* 19, 467-473.
- Zimmerman, B.E., Cessna, J.T., 2000. "Experimental determinations of commercial 'dose calibrator' settings for nuclides used in nuclear medicine." *Appl. Radiat. Isot.* 52, 615-619.
- Zimmerman, B.E., Collé, R., Cessna, J.T., 2004. "Construction and implementation of the NIST triple-to-double coincidence ratio method (TDCR) for the standardization of radionuclides." *Appl. Radiat. Isot.* 60, 433-438.

Table 1 Details of the nuclear decay data used in the analysis of experimental data. All data were taken from the DDEP evaluation (all by A.L. Nichols) indicated. The activity ratios expected at secular equilibrium ($A/A_{\text{Ra-224}}$) were calculated from the Bateman equation using the DDEP half-lives. Uncertainties ($k = 1$) on the activity ratios are calculated from the nuclear data (Bé et al., 2004; DDEP, 2018) uncertainties and owe mostly to the uncertainties on the ^{212}Pb half-life and the ^{212}Bi α/β branching ratio.

Nuclide	Evaluation Date	$T_{1/2}$	$A/A_{\text{Ra-224}}$
^{224}Ra	April 2010	3.631(2) d	1
^{220}Rn	April 2010	55.8(3) s	1.000178(1)
^{216}Po	May 2010	0.148(4) s	1.000178(1)
^{212}Pb	May 2010	10.64(1) h	1.13928(15)
^{212}Bi	May 2010	60.54(6) min	1.15263(15)
^{212}Po	May 2010	300(2) ns	0.7385(11)
^{208}Tl	July 2010	3.058(6) min	0.4144(20)

Table 2 Simplified decay schemes for the beta-emitting progeny of ^{224}Ra used in MICELLE2 efficiency calculations. Transition labels are consistent with the DDEP level schemes (DDEP, 2018). Branch probabilities (P_{br}) are renormalized such that “missing” decays are assigned to energetically similar cascades.

Daughter nuclide	beta-gamma transitions					
	A	P_{br}	B	P_{br}	C	P_{br}
^{212}Pb	$\beta_{0,3}$ $\gamma_{3,1}$ $\gamma_{1,0}$	0.0499	$\beta_{0,2}$ $\gamma_{2,0}$	0.817	$\beta_{0,0}$	0.1331
^{208}Tl	$\beta_{0,2}$ $\gamma_{2,1}$ $\gamma_{1,0}$	0.492	$\beta_{0,3}$ $\gamma_{3,1}$ $\gamma_{1,0}$	0.221	$\beta_{0,4}$ $\gamma_{4,2}$ $\gamma_{2,1}$	0.287

Table 3 TDCR uncertainty budget.

TDCR Uncertainty Component	%		
	E2	E3	E4
Counting statistics; combination of the within insertion (0.14 %; estimated as the typical standard deviation on repeat measurements for a single source, single insertion ($N = 2$ to 400)) and between insertion (0.02 %; estimated as the typical standard deviation on repeat insertions of a single source with a single gray filter ($N = 2$ to 3)).	0.15	0.27	0.21
Model uncertainty (efficiency variation); estimated as the typical standard deviation on measurements of a source with ($N = 4$) different gray filters.	0.09	0.07	0.07
Between source; estimated as the standard deviation on the activity concentration obtained with ($N = 3$) LS sources.	0.04	0.33	0.04
Background	0.04	0.03	0.002
Ra-224 half-life; propagation of the standard uncertainty on the DDEP half-life for ^{224}Ra (3.631(2) d) (Bé et al., 2004; DDEP, 2018).	0.001	0.04	0.07
Nuclear data: combination of estimated uncertainty due to the half-lives and branching ratios of ^{224}Ra and its progeny at equilibrium predicted by the Bateman Equation (dominated by uncertainty on ^{212}Bi decay branching ratio); uncertainty due to beta shape and endpoint uncertainties; uncertainty due to missed coincidences in the $^{212}\text{Bi}+^{212}\text{Po}$ decay	0.13	0.13	0.13
Efficiency Model (quenching model); propagation of an estimated uncertainty on the Birks parameter ($kB = 0.0075(15)$ MeV/cm)	0.02	0.02	0.02
Mass determinations	0.05	0.05	0.05
Combined standard uncertainty ($u_c = (\sum u_i^2)^{1/2}$)	0.23	0.46	0.27

Table 4 CNET uncertainty budget.

CNET uncertainty component	%	
	E2	E3
LS measurement precision; reproducibility in massic activity for 1 cocktail composition in E2 and 2 compositions in E3, with 6 samples each, measured in 2 counters on 4 measurement occasions in E2 and 3 occasions in E3; standard deviation of the mean for $N = 4$ data sets for E2, $N = 3$ for E3, normally distributed. The LS within-measurement precision for a given data set, in terms of the standard deviation of the mean for 6 samples measured for 5 to 10 cycles on multiple measurement occasions, ranged from 0.15 % to 0.56 %.	0.12	0.37
Background; wholly embodied in LS measurement precision	--	--
LS counters dependencies; wholly embodied in component LS measurement precision	--	--
Mass determinations	0.05	0.05
Live time determinations for LS counting time intervals, includes uncorrected dead time effects	0.06	0.06
Massic activity of ^3H (for uncertainty in standard of 0.96 %)	0.005	0.005
Ra-224 half-life (from DDEP, 3.631(2) d)	0.04	0.05
H-3 half-life (from DDEP, 12.312(25) a)	0.0001	0.0001
Computed β detection efficiencies (model dependencies and computed β spectra)	0.30	0.30
Combined standard uncertainty ($u_c = (\sum u_i^2)^{1/2}$)	0.33	0.52

Table 5 Activities calculated by linear extrapolation of data acquired during E2 with three different gates (see Figure 8) and with a weighted combination of gates, $Y_{\text{eff}} = 0.29*Y_1 + 0.67*Y_2 + 0.04*Y_3$. Correcting the intercepts by factors calculated from the Monte Carlo (MC) simulations improves accord, as shown by the reduced standard deviation (*sd*) in the second row. The activities were normalized relative to the activity calculated from the Monte Carlo-corrected Y_{eff} extrapolation (shown in bold).

	Y_1	Y_2	Y_3	Y_{eff}	avg	<i>sd</i>
no MC	1.0009	0.9956	0.9969	1.0008	0.99855	0.00271
MC	0.9988	0.9975	0.9983	1.0000	0.99863	0.00107

Table 6 LTAC uncertainty budget.

LTAC uncertainty component	%	
	E2	E3
Counting statistics: Typical standard deviation of the mean for repeated activity determinations ($N = 4$ to 47) on a single source on a single measurement (0.10 % in E2, 0.07 % in E3) combined with the typical standard deviation for repeated activity determinations ($N = 2$ to 3) on a single source on different occasions (0.25 % in E2, 0.05 % in E3)	0.26	0.09
Between source: Standard deviation on the activities determined for 3 sources	0.02	0.26
Model uncertainty: Estimated as a combination of the difference between quadratic and linear extrapolations, the standard deviation on activities determined via linear extrapolation of six different inefficiency domains, and the uncertainty on the Monte Carlo correction ($f = 0.9993(1)$).	0.07	0.07
Mass determinations	0.05	0.05
Live Time: Estimated based on previous work	0.10	0.10
Background: Estimated by propagating the standard deviation of the mean for repeated measurements of the matched blank	0.01	0.12
Impurities: no photon-emitting impurities observed	-	-
Decay correction: Propagation of the ^{224}Ra half-life uncertainty	0.002	0.04
Nuclear data: Estimated uncertainty due to the half-lives and branching ratios of ^{224}Ra and its progeny at equilibrium predicted by the Bateman Equation (dominated by uncertainty on ^{212}Bi decay branching ratio)	0.02	0.02
Combined standard uncertainty ($u_c = (\sum u_i^2)^{1/2}$)	0.30	0.33

Table 7 Comparison of methods and experiments. Within each experiment (E2, E3, and E4), results are normalized to TDCR. The VIC results are normalized by the K_{VIC} determined in E2 to provide an experiment-to-experiment comparison.

	E2		E3		E4	
	A / A_{TDCR}	u_c	A / A_{TDCR}	u_c	A / A_{TDCR}	u_c
TDCR	1	0.0023	1	0.0046	1	0.0027
LTAC	1.0023	0.0030	0.9998	0.0033		
CNET	0.9967	0.0033	1.0062	0.0050		
AutoIC*	0.9983	0.0001	0.9981	0.0009	1.0002	0.0002
GWC**	1.0003	0.0034				
HPGe***	0.9614	0.0222	0.9460	0.0141		
VIC	1	0.0024	0.9984	0.0047	0.9997	0.0036

* The AutoIC activities given here are based on the theoretical K_{AIC} ; the stated uncertainties are based on the standard deviation of repeat determinations of the ratio of the ^{224}Ra source current to RRS current and do not include model uncertainties (estimated as 1.4 %).

** The gamma well counter (GWC) activity given here is based on the theoretical response of a NaI(Tl) well counter calculated by Monte Carlo. The stated uncertainty is based on the standard deviation of repeat measurements and does not include model uncertainties (conservatively estimated as 3 %).

*** The HPGe activities given here were based on the emission probability (P_g) for the 241 keV gamma-ray according to the DDEP evaluation for ^{224}Ra . The consistent bias suggests that the P_g may require revision.

Table 8 Dial settings (*DS*) determined by the calibration curve method to give the correct activity for 5 mL of a 1 mol/L HCl solution of ^{224}Ra in equilibrium with its progeny in a NIST standard 5 mL flame-sealed ampoule. Uncertainties on the dial settings are given in parentheses and are expanded ($k = 2$) uncertainties. The resulting relative expanded uncertainty on the measured activity (U_A) is given in the last column.

model	<i>DS</i>	$U_A / \%$
CRC-15R	739(9)	1.1
CRC-35R	745(15)	1.4
CRC-25PET	737(9)	0.8
CRC-55tR	736(8)	0.9
CRC-55tPET	732(7)	0.7

Table S1 AutoIC uncertainty budget.

AutoIC uncertainty Component	%
TDCR activity: typical standard uncertainty from 3 experiments	0.30
Measurement: typical standard deviation of the mean on between 4 and 38 current ratio measurements spanning up to 1 d	0.03
Typical ²²⁴ Ra half-life (from DDEP, 3.631(2)d)	0.01
Typical Weighing	0.05
Between-experiment	0.07
Combined standard uncertainty ($u_c = (\sum u_i^2)^{1/2}$)	0.31

Table S2 VIC uncertainty budget.

VIC uncertainty Component	%
TDCR activity	0.30
Measurement: combination of the typical within- and between-insertion variance for a single source and the typical between-source variance	0.09
Ra-224 half-life (from DDEP, 3.631(2) d)	0.01
Weighing	0.05
Between-experiment	0.05
Combined standard uncertainty ($u_c = (\sum u_i^2)^{1/2}$)	0.32

Fig.1 Decay chain of ^{224}Ra and progeny to stable ^{208}Pb . Half-life data are taken from (DDEP, 2018).

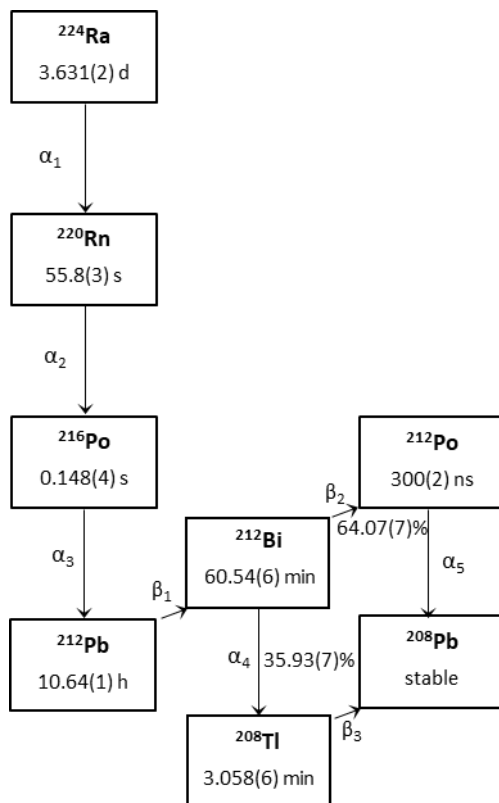


Figure 2 (A) Logical sum of doubles count rate, N , as a function of the coincidence resolving time (τ). Data were acquired with the darkest available gray filter in order to reduce the total counting efficiency. (B) Normalized data showing the count rates relative to the data obtained with $\tau = 150$ ns; at 500 ns, a slight increase is evident, perhaps due to random coincidences. With $20 \leq \tau < 500$ ns, count rates did not vary with τ , indicating that the assumption that all ^{212}Po decays are detected with ^{212}Bi is valid. The red circle corresponds to $\tau = 150$ ns, the setting used in the activity determinations (color online).

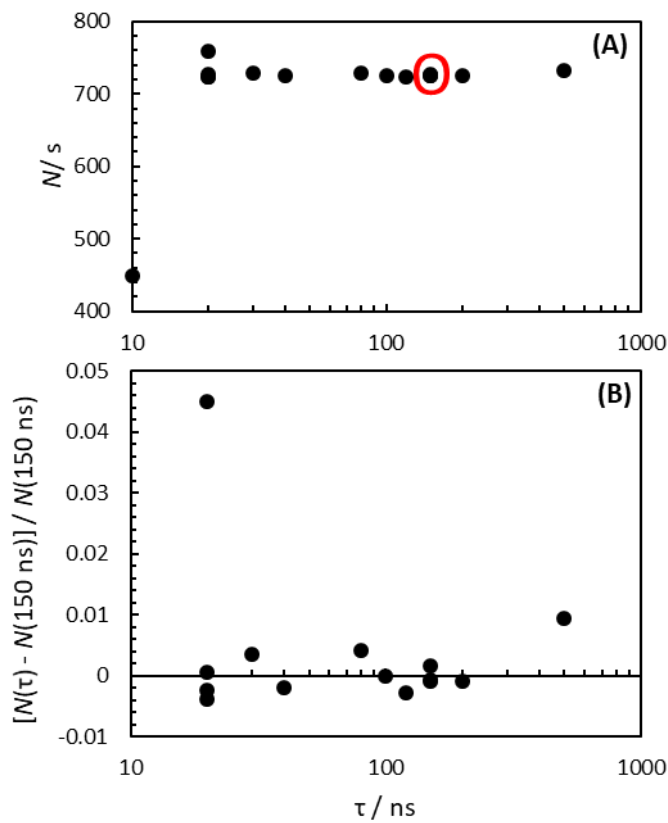


Figure 3 NaI(Tl) spectrum obtained with a ^{224}Ra source at secular equilibrium. The black solid trace is experimental data acquired in the γ -ray channel of the LTAC. The gray dashed trace is from a Monte Carlo simulation. The anticoincidence gate settings are shown as red boxes (color online).

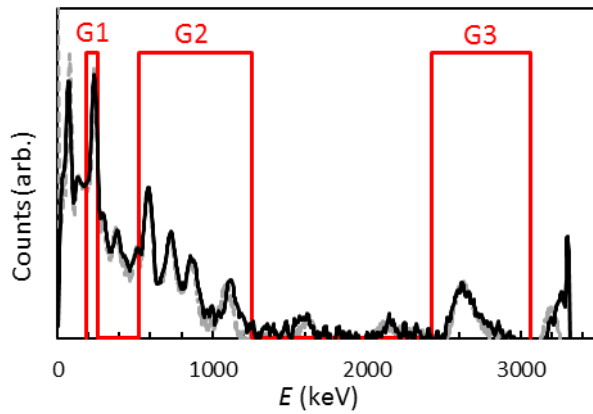


Figure 4 (A) LS channel count rates, N_{LS} , as a function of inefficiency, Y . The black, red, and gray data correspond to data acquired with G1, G2, and G3, respectively (color online).

Efficiency variation is achieved by increasing the lower-level discriminator threshold for the LS channel. (B) Extrapolations over linear regions give convergent intercepts at $Y = 0$, where the count rate is nearly equivalent to the sum of the Bateman coefficients for ^{224}Ra and its progeny (minus ^{212}Po , which is counted with ^{212}Bi —see Section 2.2.1 and Figure 2). The solid blue line represents the weighted combination of gates, $Y_{\text{eff}} = 0.29*Y_1 + 0.67*Y_2 + 0.04*Y_3$.

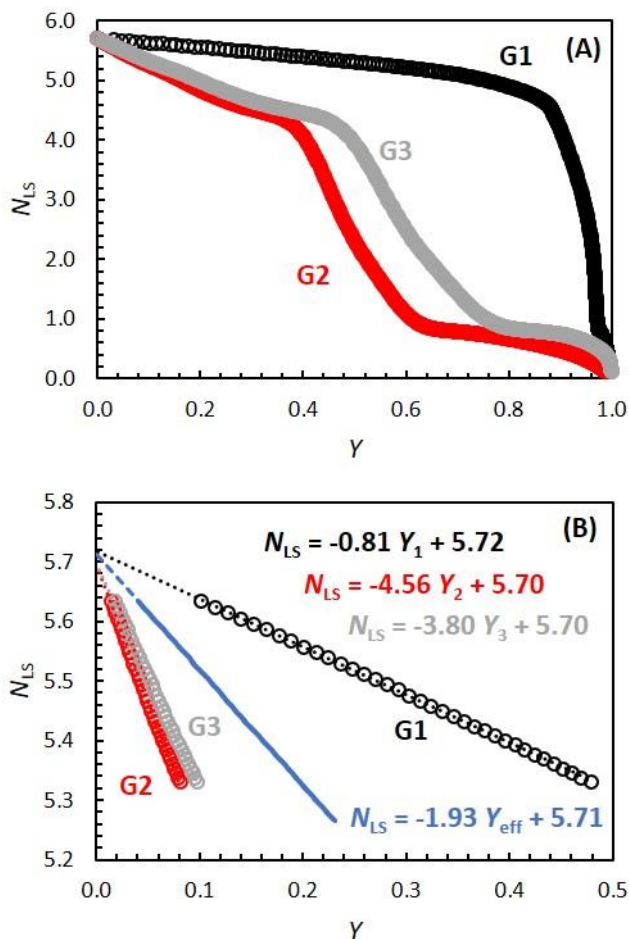


Figure 5 Decay-corrected (using the ^{224}Ra half-life) ionization chamber response, normalized by solution mass, plotted against time (with an arbitrarily set reference time). One of the ampoules (A2) was opened and transferred twice (generating A2-T1, then A2-T2). The transfers did not affect the response, indicating that loss-free transfers were possible using a 1 mol/L HCl solution. The uncertainty bars correspond to standard deviations of the mean on 200 repeated current measurements (color online).

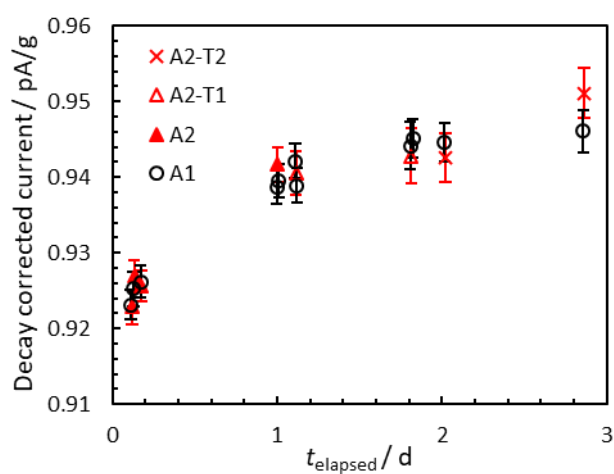


Figure 6 TDCR-determined (black open circles) and CNET-determined (red open triangles) activities from E3, normalized by the TDCR activity, for Ultima Gold cocktails as a function of time since separation. (Color online.)

